High thermoelectric performance of graphite nanofibers

Van-Truong Tran[1, #*], Jérôme Saint-Martin[2], Philippe Dollfus[2] and Sebastian Volz[1, 3]

[1]EM2C, CentraleSupélec, Université Paris Saclay, CNRS, 92295 Châtenay Malabry, France
[2]C2N, CNRS, Université Paris-sud, Université Paris Saclay, 91405 Orsay, France
[3]LIMMS, Institute of Industrial Science, University of Tokyo, CNRS-IIS UMI2820, 4-6-1 Komaba Meguro-Ku, Tokyo 153-8505, Japan
[#]Present address: SRMP, CEA Saclay, Université Paris-Saclay, F-91191, Gif-sur-Yvette, France
*vantruongtran.nanophys@gmail.com

Supporting information for methods

Density functional theory (DFT) calculations

In this work, we used the localized orbital density functional theory implemented within the SIESTA package.[1] To include the van der Waals (vdW) interactions between atoms in different layers, the pseudo-potentials were corrected by adding the DRSLL-vdW interactions[2] and generated with Atom program[3] under Troullier-Martins scheme.

All DFT calculations were performed after connecting hydrogen atoms to all edge-carbon atoms to compensate the sp2 dangling bonds[4] and thus to avoid strong edge deformation which could generate unexpected states in the gap due to the charge transfer effect. This is also consistent with the treatment of the Force Constant or Tight Binding model herein the truncation at the edges is usually considered with extended lines of carbon atoms on each side of the edges to compensate the sp2 dangling bonds of the edge carbon atoms, and these extended lines are treated as hard walls that do not impact on the results of tight binding calculations.

Additionally, in all structures, lattice vectors along *x*, *y* directions (perpendicular to the fiber axis) were set sufficient large (40 Angstrom) to avoid interactions between the system and its images because of the periodic boundary condition.

In all DFT calculations, the double Zeta polarized (DZP) orbital basis set was used and a mesh energy cutoff of 400 Ry was taken. A Monkhorst-Pack[5] 1×1×10 was chosen for the relax calculations, while for the band structure and transport studies a grid 1×1×20 was adopted. All structures were relaxed within conjugate-gradients (CG) method until the total force was less than

0.05 eV/Angstrom. The variable cell in relaxation was also set up to search for an appropriate equilibrium distance between graphite layers.

Force Constant (FC) model

For the study of phonons, we employed a Force Constant (FC) model in which the secular equation for phonons is written:

$$D\mathsf{U} = \omega^2 \mathsf{U}, \tag{S1}$$

where U is the column matrix containing the amplitude vectors of vibration at all lattice sites and ω is the angular frequency, D is the Dynamical matrix which is calculated as [6,7]

$$D = \left[D^{ij}_{3\times 3} \right] = \left[\begin{cases} -\dfrac{K_{ij}}{\sqrt{M_i M_j}} & \text{for } j \neq i \\ \dfrac{\sum_{n\neq i} K_{in}}{M_i} & \text{for } j = i \end{cases} \right] \tag{S2}$$

The coupling tensor K_{ij} between the i-th and j-th atoms is defined depending on whether the type of interaction is in-plane or inter-plane, i.e.

(i) For in-plane interactions, K_{ij} is determined by a unitary in-plane rotation [6,7]

$$K_{ij} = U^{-1}\left(\theta_{ij}\right) K^0{}_{ij} U\left(\theta_{ij}\right) \tag{S3}$$

where

$$U\left(\theta_{ij}\right) = \begin{bmatrix} \cos\left(\theta_{ij}\right) & \sin\left(\theta_{ij}\right) & 0 \\ -\sin\left(\theta_{ij}\right) & \cos\left(\theta_{ij}\right) & 0 \\ 0 & 0 & 1 \end{bmatrix} \tag{S4}$$

is the rotation matrix [7] and θ_{ij} is the anticlockwise rotating angle formed between the the *x*-axis and the vector joining the *i*-th to the *j*-th atoms. In equation (S3), K^0_{ij} is the force constant tensor that contains the force constant parameters [7]

$$K^0_{ij} = \begin{pmatrix} \Phi_r & 0 & 0 \\ 0 & \Phi_{t_i} & 0 \\ 0 & 0 & \Phi_{t_o} \end{pmatrix} \quad \text{(S5)}$$

where Φ_r, Φ_{t_i}, and Φ_{t_o} are the force constant coupling parameters in the radial, in-plane and out-of-plane directions, respectively, and their values usually decay with the neighboring distance. In this work, a four nearest neighbor range was considered and thus twelve parameters for in-plane coupling was taken from Ref.[8].

(ii) For the vdW or interlayer interactions, we employed the spherically symmetric interatomic potential model, in which each component of the coupling tensor K_{ij} is defined by:[9]

$$\left(K_{ij}\right)_{kk'} = \delta\left(r^{ij}\right).\frac{r^{ij}_{k}.r^{ij}_{k'}}{\left(r^{ij}\right)^2} \quad \text{(S5)}$$

with $k, k' = \overline{1,3}$ or x, y, z . r^{ij} is the vector joining the *i*-th to the *j*-th atoms and $\delta\left(r^{ij}\right)$ is the decaying component $\delta\left(r^{ij}\right) = A.\exp\left(-r^{ij}/B\right)$ with empirical parameters $A = 573.76$ N/m, $B = 0.05$ nm. It should be noted that equation (S5) does not contain the minus sign "-" as in ref. [9] because this sign has been included in equation (S2). Moreover, to have the best fit between the FC model and the experimental data for bulk graphite, in the FC model the distance between two graphite layers was taken equal to 0.328 nm.

Green's function formalism for transport study

To study the transport properties of both electrons and phonons, the atomistic Green' function formalism was employed.[10] All device structures were divided into three parts: the left and right leads and the device region (central region). The leads were treated as semi-infinite regions while

the central region is a finite region containing the left lead extension, the active region, and the right lead extension. In our calculations, the left (right) lead extension was chosen of the size of one unit cell (6.56 Angstrom) that is enough to make the left (right) lead isolated from the active region. The active (or scattering) region contains N_A unit cells with the length $L_A = N_A \times a_z$ where $a_z \approx 0.656$ nm.

The Hamiltonian H or the Dynamical matrix and the overlap matrix S of the whole device structure were split into three parts H_L, H_D, H_R and S_L, S_D, S_R (similarly D_L, D_D, D_R for phonons) as the Hamiltonians and overlap matrices of the left lead, device part(central region) and right lead, respectively, including the couplings between the device and the two leads H_{DL}, H_{DR}, S_{DL}, and S_{DR} (D_{DL}, D_{DR} for phonons). The Green's function of the device region is defined by the equation

$$G = \left[\left(E + i.\eta \right).S_D - H_D - \Sigma^s{}_L - \Sigma^s{}_R \right]^{-1}, \tag{S6}$$

where η is a positive infinitesimal number and

$$\begin{aligned} \Sigma^s{}_L &= \left(E^+.S_{DL} - H_{DL} \right) G^0{}_L \left(E^+.S_{LD} - H_{LD} \right) \\ \Sigma^s{}_R &= \left(E^+.S_{DR} - H_{DR} \right) G^0{}_R \left(E^+.S_{RD} - H_{RD} \right) \end{aligned} \tag{S7}$$

are the surface self-energies describing the energy-dependent coupling with the left and right leads. $G^0{}_{L(R)}$ is the surface Green's function of the isolated left (right) lead.[11,12]

For phonons, we just need to replace energy E by ω^2, and H_D, H_{DL}, H_{LD}, H_{DR}, H_{RD} by D_D, D_{DL}, D_{LD}, D_{DR}, D_{RD}, respectively. We also set $S_D = \mathbf{1}, S_{DL} = S_{LD} = S_{DR} = S_{RD} = \mathbf{0}$ for phonons.

The size of the device Green's function was reduced by making use of the recursive technique. [13,14] The electron (phonon) transmission was computed as [15]

$$T_{e(p)} = Trace \left\{ \Gamma^s{}_L \left[i \left(G_{11} - G_{11}{}^\dagger \right) - G_{11} \Gamma^s{}_L G_{11}{}^\dagger \right] \right\}, \tag{S8}$$

where $\Gamma^s_{L(R)} = i \left(\Sigma^s_{L(R)} - \Sigma^s_{L(R)}{}^\dagger \right)$ denotes the surface injection rate at the left (right) lead.

The electrical conductance, the Seebeck coefficient and the electron thermal conductance were computed within the Landauer-Onsager's approach, i.e,[16]

$$\begin{aligned} G_e(\mu,T) &= e^2.L_0(\mu,T) \\ S(\mu,T) &= \frac{1}{e.T}.\frac{L_1(\mu,T)}{L_0(\mu,T)} \\ \kappa_e(\mu,T) &= \frac{1}{T}.\left[L_2(\mu,T) - \frac{L_1(\mu,T)^2}{L_0(\mu,T)}\right] \end{aligned} \tag{S9}$$

where the intermediate functions L_n may be written in the form [6,15,17]

$$L_n(\mu,T) = \frac{1}{h}\int_{-\infty}^{+\infty} dE.T_e(E).(2K_bT)^{n-1}.g^e{}_n(E,\mu,T), \tag{S10}$$

where $g^e{}_n(E,\mu,T) = \left(\frac{E-\mu}{2K_bT}\right)^n / \cosh^2\left(\frac{E-\mu}{2K_bT}\right)$ is a dimensionless function and K_b is the Boltzmann constant.

Similarly, the Landauer-like formula was used to compute the phonon thermal conductance [15,16]

$$K_p = \frac{K_b}{2\pi}\int_0^{\infty} d\omega.\mathrm{T}_p(\omega).g^p(\omega,T), \tag{S10}$$

where $g^p(\omega,T) = \left(\frac{\mathrm{h}\omega}{2K_bT}\right)^2 / \sinh^2\left(\frac{\mathrm{h}\omega}{2K_bT}\right)$ is also a dimensionless function, as $g^e{}_n(E,\mu,T)$.

Finally, to assess the thermoelectric ability of a structure, the figure of merit ZT is used as the essential criterion and is calculated as [6,18,19]

$$ZT = \frac{G_e.S^2}{K_e + K_p}.T \tag{S10}$$

The electronic relaxation and band structure calculations were performed within the SIESTA module while the electron transmission was implemented with TransSIESTA module of the SIESTA package. The Force Constant model and Green's function technique for phonons were treated within our house-made code. We also used the Virtual Nanolab (VNL) [20] as a graphic user interface for the SIESTA code.

Supporting information for additional results

To validate the FC model, we performed phonon dispersion calculations and compared the results to the experimental data of ref. [21]. Since the direction of interest in this work is along the c-axis, we focussed on the phonon bands along the GA k-path (see figure S1(b)). As it can be seen in figure S1(c), the solid black lines obtained from the FC model are in excellent agreement with the experimental data, demonstrating the quality of this model.

Remarkably, the phonon frequency range along the c-axis is much shorter than along other axes [21], confirming that the vdW interaction between graphite layers is very weak.

In figure S2, the phonon conductance of the structure [$M_A = 6, M_Z = 10$] with 50% isotope doping is presented. It also exhibits a similar trend as in the structure [$M_A = 4, M_Z = 5$] with a suppression of K_p in longer devices.

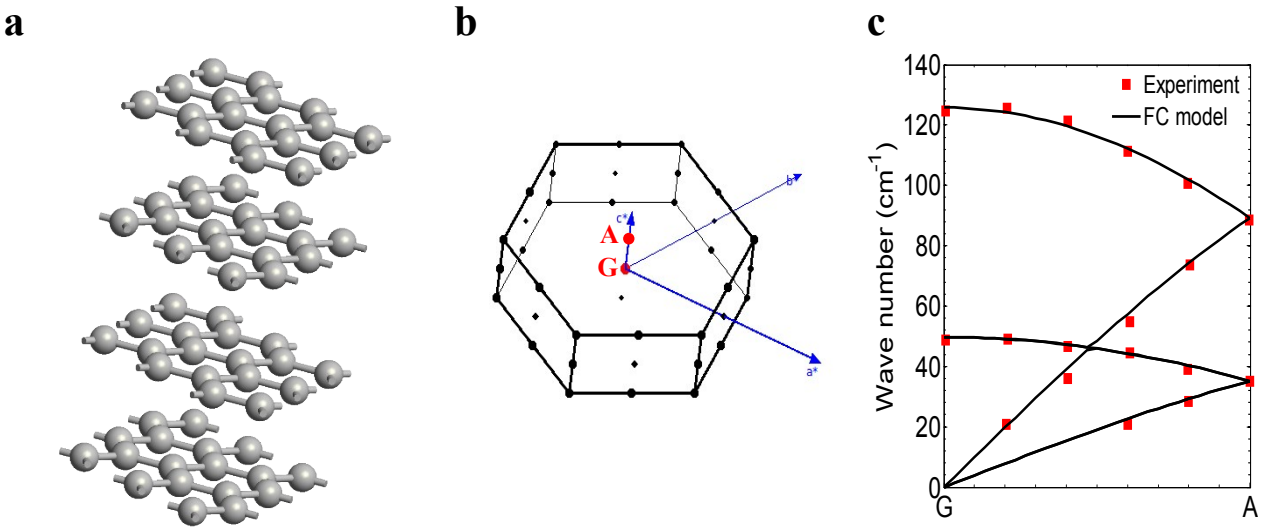

Figure S1. (a) Example of 3x3x2 unit cells of bulk graphite. (b) Brillouin zone of bulk graphite, generated using the Xcrysden software.[22] (c) Validation of the FC model for graphite by comparison with the experimental data of ref. [21].

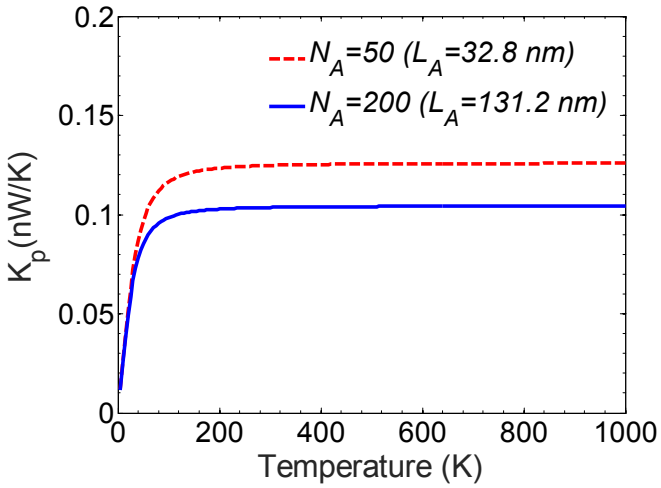

Figure S2. Phonon conductance as a function of temperature obtained for the structure of cross-section [$M_A = 6, M_Z = 10$].

References

1 J. M. Soler, E. Artacho, J. D. Gale, A. Garcia, J. Junquera, P. Ordejon and D. Sanchez-Portal, *J. physics. Condens. matter* , 2002, **14**, 2745.

2 M. Dion, H. Rydberg, E. Schröder, D. C. Langreth and B. I. Lundqvist, *Phys. Rev. Lett.*, 2004, **92**, 246401–1.

3 Atom program, https://departments.icmab.es/leem/siesta/Pseudopotentials/.

4 D. Gunlycke and C. White, *Phys. Rev. B*, 2008, **77**, 115116.

5 H. J. Monkhorst and J. D. Pack, *Phys. Rev. B*, 1976, **13**, 5188–5192.

6 V.-T. Tran, J. Saint-Martin and P. Dollfus, *Nanotechnology*, 2015, **26**, 495202.

7 M. S. D. Dresselhaus, A. Jorio, R. Saito, G. Dresselhaus, M. S. D. Dresselhaus and A. Jorio, *Physical Properties of Carbon Nanotubes*, Imperial College Press, 1998, vol. 3.

8 L. Wirtz and A. Rubio, *Solid State Commun.*, 2004, **131**, 141–152.

9 D. L. Nika, A. I. Cocemasov and A. A. Balandin, *Appl. Phys. Lett.*, 2014, **105**, 31904.

10 S. Datta, *Superlattices Microstruct.*, 2000, **28**, 253–278.

11 M. P. L. Sancho, J. M. L. Sancho and J. Rubio, *J. Phys. F Met. Phys.*, 2000, **14**, 1205–1215.

12 T. Ozaki, K. Nishio and H. Kino, *Phys. Rev. B*, 2010, **81**, 35116.

13 C. H. Lewenkopf and E. R. Mucciolo, *J. Comput. Electron.*, 2013, **12**, 203–231.

14 V.-N. Do, *Adv. Nat. Sci. Nanosci. Nanotechnol.*, 2014, **5**, 33001.

15 V. Tran, *Appendices, PhD dissertation, Université Paris-Saclay*, 2015.

16 R. D'Agosta, *Phys. Chem. Chem. Phys.*, 2013, **15**, 1758–1765.

17 V.-T. Tran, J. Saint-Martin, P. Dollfus and S. Volz, *Sci. Rep.*, 2017, **7**, 2313.

18 Abraham Fedorovich Ioffe, *Acad. Sci. USSR, Moscow*, 1950, (in Russia).

19 P. Dollfus, V. H. Nguyen and J. Saint-Martin, *J. Phys. Condens. Matter*, 2015, **27**, 133204.

20 Quantumwise, Virtual NanoLab, http://www.quantumwise.com/products/vnl#Free_VNL.

21 R. Nicklow, N. Wakabayashi and H. G. Smith, *Phys. Rev. B*, 1972, **5**, 4951.

22 A. Kokalj, *J. Mol. Graph. Model.*, 1999, **17**, 176–179.